Published in final edited form as:
Brain Struct Funct. 2014 January ; 219(1): . doi:10.1007/s00429-012-0498-y.

Tracing Superior Longitudinal Fasciculus Connectivity in the Human Brain using High Resolution Diffusion Tensor Tractography

Arash Kamali, MD[1], **Adam E. Flanders, MD**[2], **Joshua Brody, DO**[1], **Jill V. Hunter, MD**[3], and **Khader M. Hasan, PhD**[4,*]

[1]Department of Radiology, UMDNJ, Cooper University Hospital, United States of America

[2]Department of Radiology, Thomas Jefferson University Hospital, United States of America

[3]Texas Childrens Hospital, Department of Neuroradiology, United States of America

[4]University of Texas Health Science Center Houston-Medical School, United States of America

Abstract

The major language pathways such as superior longitudinal fasciculus (SLF) pathways have been outlined by experimental and diffusion tensor imaging (DTI) studies. The SLF I and some of the superior parietal lobule connections of the SLF pathways have not been depicted by prior DTI studies due to the lack of imaging sensitivity and adequate spatial resolution. In the current study, the trajectory of the SLF fibers has been delineated on five healthy human subjects using diffusion tensor tractography on a 3.0T scanner at high spatial resolution. We also demonstrate for the first time the trajectory and connectivity of the SLF fibers in relation to other language pathways as well as the superior parietal lobule connections of the language circuit using high spatial resolution diffusion tensor imaging in the healthy adult human brain.

Keywords

diffusion tensor imaging; high resolution; tractography; association fibers; superior longitudinal fasciculus

Introduction

The superior longitudinal fasciculus (SLF) is a large bundle of association fibers in the white matter of each cerebral hemisphere connecting the parietal, occipital and temporal lobes with ipsilateral frontal cortices (Schmahmann et al. 2008). The SLF facilitates the formation of a bidirectional neural network that is necessary for core processes such as attention, memory, emotions and language (Mesulam 1998; Petrides and Pandya 2002).

Five subcomponents of the SLF have been described. The superior horizontal fibers connect the superior parietal lobe (SLF-I), the angular gyrus (SLF-II) and the supramarginal gyrus (SLF-III) to ipsilateral frontal and opercular areas. The fourth component is known to be the arcuate fasciculus which connects the superior temporal gyrus and the ventrolateral prefrontal cortex together. A fifth SLF component has also been described in some prior

*Corresponding Author: Khader M. Hasan, Ph.D., Associate Professor of Diagnostic and Interventional Imaging, Department of Diagnostic and Interventional Imaging, University of Texas Medical School at Houston, 6431 Fannin Street, MSB 2.100, Houston, Texas 77030, United States of America, Tel: Office (713) 500-7690, Fax: (713) 500-7684, Khader.M.Hasan@uth.tmc.edu.

studies (Makris et al. 2005; Catani et al. 2005; Frey et al. 2008; Makris et al. 2009; Zhang et al. 2010) connecting the temporal and parietal lobes together and named temporoparietal SLF (SLF TP).

Experimental anatomical and diffusion tensor imaging (DTI) studies in non-human primates have traced various long association fiber pathways within the fronto-temporo-parietal region including the superior longitudinal fasciculus (Makris et al. 2009; Schmahmann et al. 2007; Bernal and Altman 2010; Koch et al. 2010; Rozzi et al. 2006; Petrides and Pandya 1984; Seltzer and Pandya 1984; Borra et al 2008; Luppino et al. 1999).

Diffusion tensor tractography is a technique using the diffusion tensor-MRI data to trace the compact white matter pathways noninvasively (Mori S, van Zijl 2002). Diffusion tensor tractography (DTT) allows the delineation of the location and course of the neuronal fiber tract and to elucidate its trajectory. This technique may provide information about anatomical connectivity between distant brain areas, as well as the course, interruption, or integrity of neural pathways. This information may be helpful in exploring lesion localization and specific connections that are impaired (Galantucci et al. 2011).

Details of brain white matter connectivity have been undetectable or poorly detectable due to both the discrepancy of scale between microstructural anatomy and image resolution and inadequate sensitivity in DTI. For example, several DTI studies have attempted to trace the SLF fibers on human and non-human primates. However, depiction of delicate axonal fibers of superior longitudinal fasciculi, specifically the SLF I and superior parietal lobule connections (Brodmann area 7) of the language pathways (MdLF-SPL and SLF TP-SPL) were not feasible in the human brain in previous DTI studies (Galantucci et al. 2011; Makris and Pandya 2009).

This work aimed to explore the acuity and feasibility of mapping the SLF and superior parietal lobule connections of the language pathways using a recently described high resolution DTI protocol and deterministic tractography methods (Hasan et al. 2009; Kamali et al 2010). The high spatial resolution DTI data allowed visualization of the connectivity of previously undepicted association fiber tracts of the human brain such as the SLF I and MdLF. We also provide more details on the connectivity and microstructural characteristics of the SLF in relation to other suspected language pathways.

Materials and Methods

Study Subjects

This work was approved by our institutional review board (IRB) and was health insurance portability and accountability act (HIPAA) compliant. Five right-handed healthy men (age range 24–37 years) were included in this study and written informed consent was obtained from all the subjects.

Conventional MRI Data Acquisition

All MRI studies were performed on a 3T Philips Intera scanner with a dual quasar gradient system with a maximum gradient amplitude of 80 mT/m, maximum slew rate 200 mT/ms/m, and an eight channel SENSE-compatible head coil (Philips Medical Systems, Best, Netherlands). The conventional MRI (cMRI) protocol included axially prescribed 3D spoiled gradient echo imaging (repetition time, TR = 8 ms; echo time, TE = 4ms) with a square field-of-view (FOV) = 256 mm × 256 mm and a matrix of 256×256 pixels. The slice thickness for the MRI sequences was 1.0 mm with 120 contiguous axial slices covering the entire brain from foramen magnum to vertex (Hasan and Narayana 2003).

DTI Data Acquisition

Diffusion-weighted image (DWI) data were acquired axially from the same graphically prescribed cMRI volumes using a single-shot multi-slice 2D spin-echo diffusion sensitized and fat-suppressed echo planar imaging (EPI) sequence, with the balanced Icosa21 tensor encoding scheme (Hasan and Narayana 2003). The b-factor = 500 sec mm^{-2}, TR/TE = 14460/60 msec. The spatial coverage for DTI data matched the 3D cMRI spatial coverage (FOV = 256 mm × 256 mm and slice thickness / gap/ #slices = 1 mm / 0 mm / 120). The EPI phase encoding used a SENSE k-space undersampling factor of two, with an effective k-space matrix of 112×112 and an image matrix after zero-filling of 256×256. The acquisition spatial resolution for DTI data was ~ 2.29mm × 2.29mm × 1mm, and the digitally interpolated resolution after k-space image construction was 1mm × 1mm × 1mm. The number of b-factor ~ 0 (b_0) magnitude image averages was four. The DTI acquisition was ~ seven minutes and was repeated three times to enhance signal-to-noise ratio (SNR) for a total of 21 minutes. The selection of the b-factor, parallel imaging, repetition and echo times enabled entire brain coverage using single-shot and interleaved EPI. The thin slice acquisition in space and replication of data in time combined with the DTI encoding provided several quality control options to study signal-to-noise ratio (SNR) and partial volume effects on the DTI tracking results (Hasan et al. 2008). The SNR in the non-diffusion weighted data was ~ 25–30. The SNR was computed from the b0 volumes by averaging the three data sets to compute the mean and by subtracting the volumes to compute the standard deviation (Hasan and Narayana 2003).

White Matter Fiber Tracking

After data preparation and quality assessment using in-house developed procedures, compact WM fiber tracking was performed using DTI Studio software (Johns Hopkins University, Baltimore, Maryland; http://cmrm.med.jhmi.edu/). Fiber tracking was based on the fiber assignment by continuous tracking (FACT) algorithm with a fractional anisotropy threshold of 0.22 and angle threshold of 60 degrees. Reproducibility of the fiber construction in both hemispheres was tested by two experienced raters on all subjects. Two ROIs were applied to obtain each fiber tract and an “AND” operation was performed to include the fibers passing through both of the ROIs. The T1 weighted volumes were co-registered with the DTI-derived maps on all five subjects allowing better characterization of the anatomic landmarks for placement of the ROIs using FA-modulated or color coded principal eigenvector maps. Once a fiber tract was reconstructed, the entire trajectory was verified on a slice by slice basis to ensure consistency with established anatomical landmarks based on an atlas of anatomy (Makris et al.2009; Hains 2007). The trajectory of each tract was assessed by two experts in tractography. A consensus was reached when there was not agreement on the anatomical location of the region of interests.

Fiber Tracking Regions-of-Interest

Superior longitudinal fasciculus I—The locations of the ROIs selected for each pathway are shown in Fig. 1 on one of the subjects. The corresponding coronal and axial levels are illustrated on a midsagital T1-weighted image in Fig. 2. In the coronal plane the SLF I (Fig. 1a) is first delineated over the green association bundles just superolateral to the cingulum on the DTI color coded map at the most posterior part of the corpus callosum (coronal plane c on Fig. 2). The second ROI was placed over the fibers generated on the superolateral aspect of the cingulum at the coronal plane passing though the mid thalamus (coronal plane a in Fig. 2).

Superior longitudinal fasciculus II—For delineating the SLF II (Fig. 1b) the first ROI was selected on the coronal plane at the origin of the marginal ramus of the cingulate sulcus

(the arrow on Fig. 2) over the white matter of the angular gyrus (coronal plane e on Fig. 2). The second ROI was placed on the fibers generated on the periventricular green association area of the coronal plane passing through the posterior-most portion of the fornix in the midline (coronal plane b on Fig. 2).

Superior longitudinal fasciculus III—The first ROI for the SLF III (Fig. 1c) was selected on the periventricular green association fibers (located laterally to the blue corona radiata fibers) on the coronal plane at the posterior-most portion of the fornix in the midline (coronal plane b on Fig. 2), followed by the second ROI over the fibers generated on the white matter of the supramarginal gyrus on the coronal plan passing through the marginal ramus of the cingulate sulcus (coronal cut d on Fig. 2).

Arcuate fasciculus (AF)

Delineation of the AF (Fig. 1d) was pursued by placing the first ROI on the periventricular green association white matter of the color coded map (located laterally to the blue corona radiata fibers) on the coronal plane at the posterior-most portion of the fornix in the midline. The second ROI was seeded on the craniocaudlly oriented fibers passing through the periventricular blue fibers of the axial plane at the axial level of the anterior commissure (axial level B on Fig. 2).

Temporoparietal SLF (inferior parietal lobule connection SLF TP-IPL)

The first ROI for the SLF TP-IPL (Fig. 1e) was selected on the periventricular blue fibers lateral to the green association fibers at the axial level passing through the anterior commissure (axial level B on Fig. 2) followed by seeding the second ROI on the fibers generated on the inferior parietal lobule (coronal level e on Fig. 2).

Temporoparietal SLF (superior parietal lobule connection; SLF TP-SPL)

The SLF $TP_{(SPL)}$ (Fig. 1f) was traced by seeding the first ROI on the ascending blue fibers lateral to the green association fibers at the axial level passing through the anterior commissure (axial level B on Fig. 2) and adding the second ROI on the fibers generated at the centrum semiovale.

MdLF

The superior parietal gyrus connection of MdLF ($MdLF_{(SPG)}$) (Fig. 1g) was delineated by placing the first ROI on the ascending blue fibers of the parietal cortex at axial level A on Fig. 2 and seeding the second ROI on the fibers generated in the superior temporal gyrus on the coronal plane b in Fig. 2. The angular gyrus connection of the MdLF (MdLF-AG or IPG) (Fig. 1h) was traced by seeding the first ROI on the superior temporal gyrus on coronal plane b on Fig. 2, followed by placing the second ROI on the fibers generated at the parietooccipital confluence on the coronal plane f on Fig. 2.

Other association pathways

We used the ROIs described in prior DTI studies for delineation of the inferior longitudinal fasciculus, inferior fronto-occipital fasciculus, uncinate fasciculus (Catani et al. 2002) and extreme capsule (Makris and Pandya 2009). A brief description of some of these pathways is provided here.

Extreme capsule (EmC)

The EmC is a long association fiber pathway, which courses from the inferior frontal region medially to the insula and laterally to the claustrum and inserts into the superior temporal gyrus (Makris et al. 2009).

The Inferior longitudinal fasciculus (ILF)

This pathway connects the temporal and the occipital lobes together. It covers the inferior frontooccipital fasciculus in most of the occipital white matter and these two pathways insert into the occipital lobe.

The Inferior Fronto-occipital fasciculus (IFOF)

The IFOF is the longest association pathway of the brain which connects the frontal lobe to the occipital lobe. The IFOF merges with the frontal projections of the uncinate fasciculus as well as the frontal projections of the extreme capsule in the frontal lobe. The IFOF fibers pass through the external capsule before coursing within the occipital lobe. As the IFOF courses in the occipital lobe, it is covered by the inferior longitudinal fasciculus.

The Uncinate Fasciculus (UF)

The UF courses at the bottom of the Sylvian fissure and connects the inferior frontal gyrus with the anterior temporal lobe. The UF frontal projections merge with the inferior fronto-occipital fasciculus.

The Cingulum (Cing)

Passing through the core of the cingulate and parahippocampal gyri to nearly complete a circle this tract connects the prefrontal cortex and cingulate gyrus to the hippocampus.

Results

In the present study, the trajectory of the SLF fibers was delineated in five healthy adults using diffusion tensor tractography. Except for minor variation, the basic course of the SLF in all ten hemispheres appears to be equivalent. SLF fibers were traced bilaterally on all subjects. However, in two of the subjects we were unable to trace the AF in the right hemisphere. This asymmetry has also been reported in previous DTI studies (Lebel and Beaulieu 2009; Liu et al. 2010; Dubois et al. 2009). We employed deterministic DTI tractography to reconstruct the SLF subcomponent volumes and their corresponding DTI average values.

Quantitative Analyses of the white matter Fiber Tracts

Table 1 summarizes the mean and standard deviation values of the SLF and MdLF (IPL and SPL) tract volumes and corresponding fractional anisotropy (FA) and means diffusivity (MD) in the left and right hemispheres. The difference between left and right SLF average values is indicated by the p value which was obtained using paired t-test. Note that the TP SLF volume ($p = 0.06$; Mann-Whitney non-parametric test) and corresponding fractional anisotropy was leftward asymmetric ($p = 0.05$). The fractional anisotropy was also leftward asymmetric for MdLF SPL ($p = 0.05$). The total SLF volume was ~ 4.28% of the total white matter volume (Table 1).

Qualitative Analyses of Tractograms

Superior longitudinal fasciculus (SLF)—The SLF is composed of five distinct components SLF I, SLF II, SLF III, TP SLF and arcuate fascicle (AF). Below we provide

details of our tractography results for the SLF subcomponents (Fig. 3–5). Please attention that the color-coding is fixed across all the images. We also describe the SLF pathways with respect to the middle longitudinal fasciculus, inferior longitudinal fasciculus, extreme capsule and cingulum. The trajectory of all traced pathways and their relationship with each other are portrayed in Fig. 5.

Superior longitudinal fasciculus one (SLF I)—The SLF I (light blue fibers in Fig. 5a–d) originates in the superior and medial parietal cortex, located in close proximity in the superior-lateral cingulum bundle (yellow fibers in Fig. 5a–d) on the coronal planes in each cerebral hemisphere. The SLF I extends from the superior parietal lobule along the cingulate gyri in the superior parietal and frontal white matter (Brodmann area (BA) 7, 5, 4) rostrally to the superior frontal gyrus white matter, and terminates in the dorsal and medial cortex of the frontal lobe in the supplementary (M II) (Schmahmann et al. 2008; Hains 2007) and premotor areas of the frontal lobe (BA 6, 8, and 9) (Fig. 5a–e).

Superior longitudinal fasciculus two (SLF II)—The SLF II (pink fibers in Fig. 5a–e) is situated more laterally and occupies a space in the central core of the hemispheric WM, lateral to the corona radiata and above the insula. The SLF II originates from the posterolateral region of the parietal cortex from the WM of the angular gyrus (BA 39) (Fig. 5e) posterior to the origination of the SLF III (green fibers in Fig. 5a–d) and posterior to the craniocaudal portion of the arcuate fasciculus. The SLF II courses in the anterior-posterior direction lateral to the superior parietal lobule connections of the middle longitudinal fasciculus (MdLF-SPL) (orange fibers in Fig. 5c–d) side-by-side with the horizontal portion of the arcuate fasciculus (black fibers in Fig. 5c–e) and the SLF III, through the supramarginal gyrus (BA 40) (Fig. 5d). The SLF II course continues through the post central gyrus (BA 3, 1 and 2), the precentral gyrus (area 4), and the middle frontal gyrus (BA 6 and 46) (Fig. 4a–f) and terminates in the dorsolateral prefrontal cortex (BA 6, 8 and 46) (Fig. 5a–e).

Superior longitudinal fasciculus three (SLF III)—The SLF III (green fibers in Fig. 5a–d) is the most lateral component and originates in the supramarginal gyrus (rostral portion of the inferior parietal lobe) (Fig. 5d) rostrally related to the origination of the SLF II. The SLF III fibers then course in the sylvian opercular white matter along with the SLF II and the horizontal portion of the AF and continue into the white matter of the inferior frontal gyrus and terminates in the ventral premotor and prefrontal cortex (BA 6, and 44) (Fig. 4a–l, 5a–d).

Arcuate fasciculus (AF)

The arcuate fasciculus is part of the SLF. The AF (black fibers in Fig. 5c–e) is mapped to originate from the white matter of posterior part of the superior temporal gyrus at the temporoparietal junction and sweeps around the insula and caudal Sylvian fissure, then passes next to the fibers of the SLF II and SLF III above the Sylvian fissure and insula, and terminates in the dorsal prefrontal cortex (BA 8 and 46). The AF connects the caudal temporal lobe with the dorsolateral prefrontal cortex (Fig. 5c–e).

Temporoparietal SLF (SLF TP)

The SLF TP fibers (purple fibers in Fig. 5a–d) are craniocaudally oriented fibers which course from the posterior part of the superior temporal gyrus adjacent to the origin of the arcuate fasciculus, cranially to the superior parietal lobule (BA 7). The SLF TP (purple fibers in Fig. 4h–k) arises from the posterior portion of the superior parietal gyrus adjacent to the origination of the arcuate fasciculus. As they ascend within the core of the temporoparietal white matter, some of the fibers of the SLF TP insert into the inferior

parietal lobe (angular gyrus connections of the SLF TP; white arrows on Fig. 4h, i, k) and the rest of the fibers ascend medially to the SLF II fibers and lateral to the superior parietal lobule connection of the middle longitudinal fasciculus (MdLF-SPL) fibers and insert into the superior parietal lobule (BA 7) (Fig. 4h, 5c–d).

Middle longitudinal fasciculus (MdLF)

The red fibers are the previously described (Frey et al. 2008; Makris et al. 2009) portion of the MdLF which is connected to the angular gyrus of the inferior parietal lobule (IPL) (MdLF-IPL) (Fig. 3a–f, 5e). The MdLF-IPL is situated within the WM of the caudal inferior parietal lobule and interconnects the angular gyrus (caudal part of the inferior parietal lobule, BA 39) with the superior temporal gyrus (BA 38). The MdLF-IPL courses above the ILF (dark blue) in the temporoparietal lobes (Fig. 3a–f, 4g and 4h, 5a–e).

The orange fibers (Fig. 3a–f, 4g, i, j and 5a–d) demonstrate the higher connection of the MdLF to the superior parietal lobule (SPL, BA 7). These superior parietal lobule connections (MdLF-SPL) course above the previously described (Frey et al. 2008; Makris et al. 2009) MdLF-IPL (red fibers in Fig. 3a–f, 4g, i, j and 5a–d) and are inserted just above it on the superior temporal gyrus (BA 38). The MdLF-SPL fibers can clearly be distinguished from other adjacent fiber pathways such as the extreme capsule, the inferior longitudinal fascicle, arcuate fascicle and SLF I, II and III (Fig. 4g–j, 5a–d).

Anatomical parcellation of the aforementioned fiber tracts is illustrated on the coronal planes in Fig. 5. As illustrated in Fig. 5a, at the axial level in the mid fornix, in the frontal lobe the SLF I (light blue) is located superior-lateral to the cingulum bundle (yellow), the AF (black) is traversing above the insular cortex and medial to the SLF II (pink) and SLF III (green). In the temporal lobe the MdLF-SPL (orange) is coursing above the MdLF-IPL (red color in the superior temporal gyrus) and the ILF (dark blue in the inferior temporal gyrus). The temporal horn of the cingulum bundle is also seen in the hippocampus at this level. In Fig. 5b at mid thalamic cut the fibers continue the same course. At the most posterior coronal plane of the corpus callosum (Fig. 5c), the MdLFs and ILF bundles course medially toward the central core of the cerebral hemisphere and the SLF I starts to deviate from the parietofrontal horn of the cingulum. The SLF TP (purple) is seen originating from the superior temporal gyrus along with the AF (black) ascending through the white matter core of the temporoparietal confluence. At the coronal plane of the superior ramus of the cingulate sulcus (Fig. 5d), the SLF III fibers (green) are inserting into the supramarginal gyrus (SMG is shown by arrow). At this level the AF fibers (black) are circling around the posterior insular lobe and inserting into the junction of the temporoparietal lobes alongside the SLF TP (purple). The SLF TP is also seen to ascend along with the MdLF-SPL (orange) to the superior parietal cortex. The SLF I (light blue) is seen to insert into the marginal sulcus cortices at this point. Also noted at this coronal level is the confluence of the parietofrontal and temporal horns of the cingulum. At the coronal level passing through the angular gyrus (Fig. 5e), the SLF II fibers are inserting into the angular gyrus cortices of the parietal lobe alongside the angular gyral connections of the SLF TP (purple) (AG = angular gyrus is shown by the arrow). The MdLF-IPL (red) courses above the ILF (dark blue) in the temporoparietal lobes and both course toward the occipital cortices (Fig. 5a–e).

Discussion

The current study demonstrated for the first time the feasibility of high resolution DTI tractography to identify the anatomy and microstructural neural pathways of five distinct subcomponents of the SLF fibers which are bundled together but are functionally separate based on the known anatomical knowledge from human and non-human primates (Schmahmann et al. 2008; Rozzi et al. 2006; Petrides and Pandya 1984; Seltzer and Pandya

1984; Borra et al 2008; Luppino et al. 1999). We also reported for the first time the superior parietal lobule connections of the language pathways (MdLF-SPL and SLF TP-SPL) as well as the anatomical landmarks, ROIs for delineation, the macrostructural volumetric and corresponding microstructural attributes (such as FA and mean diffusivity) of the SLF I, SLF II, SLF III, SLF TP, MdLF and the arcuate fasciculus.

The current study presented in detail the ROIs used to parcellate the different pathways hypothesized to be involved in human language expression and comprehension. Based on our experience, tracing the SLF subdivisions highly relies on cortically-dependent ROI positioning and to the best of our knowledge, the current study is the first to present a two-seed approach for tracing the SLF fibers based on the cortical and subcortical connections of these pathways. Furthermore, we demonstrated coronal mapping of the SLF and other mentioned language pathways on anatomical images (Fig. 5) to better characterize the course and the cortical attachments of these tracts in relation to the neighboring white matter fibers. Our findings on the topography of the SLF and other pathways are consistent with previous DTI studies on primates (Schmahmann et al. 2007) as well as human neuroanatomy descriptions (Schmahmann et al. 2008, Hains 2007).

The SLF I, II, III and the AF have been anatomically traced using diffusion weighted imaging probabilistic algorithms as separate trajectories on monkey brain using long scan times (Schmahmann et al. 2007). Due to the close proximity of the SLF I and cingulum bundle and inadequate spatial resolution used in prior DTI tractographic studies, depiction of fine-scale SLF components and specifically the SLF I was not feasible. We confirmed in this study that the SLF I is distinct and measurable from the adjacent cingulum bundle. Our results correspond to the results of a prior human DTI study using the Talairach atlas for three-dimensional reconstruction of the SLF I from a series of two-dimensional outlines manually placed on coronal sections (Makris et al. 2005). A recent DTI study demonstrated the tractograpgy of the SLF I (Jang and Hong 2012). This study (Jang and Hong 2012) traced the SLF I by using the cortical ROIs only and did not represent the trajectory of the adjacent cingulum bundles that also have similar cortical connections (see Fig. 3g–l). Thus, by not delineating the SLF I and cingulum bundle on the coronal plane (as is done in the current study) there is a very high possibility of mixing the cingulum bundle cortical subtrajectories with the SLF I tract.

To the best of our knowledge the current study is the first to present a two-seed approach to trace the SLF I and demonstrate the connectivity and 3D reconstruction of the SLF I in relation to the neighboring pathways of the human brain. The SLF I is clearly discernable from the cingulum bundle. The ability to differentiate the SLF I from the neighboring cingulum bundles confirms the fact that the SLF I is an important distinct long parietofrontal white matter fiber pathway running within the superior parietal and frontal gyri connecting the important somatosensory and language cortices. The consistency of the SLF trajectories from this work with a prior probabilistic study on monkeys (Schmahmann et al. 2007) suggests that the SLF in the human brain has close similarity in structure to that in non-human primates.

Our approach also revealed the long association bundle connectivity (orange fibers on Fig. 3a–f, 4g–j) of the superior parietal lobule (BA 7) with superior temporal gyrus (BA 38) which has not been demonstrated before. We assumed that these connections should be part of the MdLF as they course side by side within the temporal lobe and have common insertion into the superior temporal gyrus (BA 38), thus we named it the superior parietal lobule connection of the middle longitudinal fasciculus (MdLF-SPL). The MdLF-SPL is clearly distinct from adjacent pathways such as the MdLF-IPL, AF and ILF or from parietofrontal association fibers such as the SLF I, II, III or EmC. We named these fibers the

MdLF-SPL as they follow the course of the previously described the MdLF-IPL from the superior temporal gyrus (BA 38) (Fig. 3a–f, 5a–c), situated superior and parallel in relation with the MdLF-IPL fibers to the confluence of the temporal and parietal lobes (Makris et al. 2009). At this point (Fig. 5c, d) the MdLF-SPL fibers instead of insertion into the angular gyrus in the inferior parietal lobule (BA 39), separate from the MdLF-IPL and rise to the superior parietal cortex (BA 7). To the best of our knowledge no connection between the superior parietal lobule and the superior temporal gyrus has been elucidated on prior experimental and anatomical studies on primates (Rozzi et al. 2006; Petrides and Pandya 1984; Seltzer and Pandya 1984; Borra et al 2008; Luppino et al. 1999) or prior DWI studies (Schmahmann et al. 2007) on monkeys.

The fifth temporoparietal component (SLF TP) is known to connect the inferior parietal lobule with the posterior part of the superior temporal gyrus at the temporoparietal junction adjacent to the insertion of the arcuate fasciculus (Catani et al. 2005 ; Schmahmann et al. 2007; Bernal et al. 2010). Despite some controversies regarding the nomenclature of this tract we included this pathway in SLF bundles as also has been described in previous studies (Makris et al. 2005; Catani and Jones 2005; Frey et al. 2008; Zhang et al. 2010; Galantucci et al. 2011).

In our experience, in addition to the previously described inferior parietal lobule connections of the SLF TP (Catani et al. 2005 ; Schmahmann et al. 2007; Bernal et al. 2010), most of these fibers project to the superior parietal lobule (BA 7) adjacent to the insertion of the aforementioned MdLF-SPL (Fig. 4h–k and 5d). These superior parietal connections of the SLF TP-SPL course medially to the SLF II and lateral to the MdLF-SPL fibers and project to the posterior portion of the superior temporal gyrus adjacent to the origination of the AF. However, the course of the currently identified superior parietal connection of the SLF TP appears similar to the previously described inferior parietal (angular gyrus) connection SLF TP (SLF TP-IPL) (Catani et al. 2005; Schmahmann et al. 2007; Bernal et al. 2010). Future studies with different techniques, combined with function and high spatial resolution probabilistic tractography may be helpful to confirm if these higher temporoparietal white matter connections are part of the previously described SLF TP or a separate newly identified temporoparietal language bundle that runs side-by-side with it and ends in the superior parietal cortex.

The superior parietal connection of the MdLF and SLF TP in human brain may provide a preliminary postulate of the potential role of the MdLF and SLF TP as language pathways within the parietotemporal circuitry of the language network. These higher parietal interconnections with superior temporal gyrus in human brain may serve a role in higher cognitive and comprehensive language functions compared with non-human primates.

Using thin 1mm DTI data along with exact ROIs based on clear anatomical landmarks, partial volume effects were dramatically reduced specifically at the white matter core of the temporoparietal confluence adjacent to the lateral ventricles where the highest load of fiber intercrossing is present. This enabled us to circumvent the intra-voxel incoherency to some limited extent and reveal the anatomical details of the SLF TP-SPL and MdLF-SPL. However, crossing fibers within a voxel remains a limitation to deterministic or FACT-based DTT using one single tensor (Barrick and Clark 2004; Jones 2008). A given DTI-based trajectory may not correspond exactly to the fine distribution of actual axonal bundles due to crossing and kissing fibers that may cause false positive or false negative results (Barrick and Clark 2004; Jones 2008). However, the consistency of the current results across all five subjects and strong correspondence with the anatomical description in the literature makes false positive results extremely unlikely.

Our data were acquired using anisotropic voxel dimensions (i.e. ~2mm×2mm×1mm interpolated in k-space to 1mm×1mm×1mm). One could argue that this will more beneficial to fiber tracking of the fiber groups that align with the direction of the higher resolution. In our experience, the thinner dimension in the axial plane was helpful in tracing the fiber tracts with a component of craniocaudal orientation such as the MdLF SPL, MdLF IPL, SLF TP-SPL and SLF TP-IPL. In addition, using the higher resolution in the axial plane helped resolve the contributions related to crossing fibers. For example, reducing the intra-voxel heterogeneity from the craniocaudally oriented fibers of the cingulum which are crossing with the SLF I fibers (anterior-posterior orientation) also helped tracking the SLF I. However, the intention of this work was not to study in detail or simulate these effects and future intra subject comparison using our method and more conventional isotropic acquisition schemes would be helpful for validation and better resolution of this issue. Furthermore, future advances in high field MRI systems and parallel image acquisition to increase signal and to reduce scan time in combination with high angular DTI methods such as diffusion spectrum imaging (Wedeen et al. 2008) may overcome some of the challenges due to crossing fibers and intra-voxel orientation heterogeneity.

The number of healthy subjects examined in this DTI study was small for a more comprehensive quantitative assessment of hemisphere, gender and age effects. For example, leftward laterality of the arcuate fasciculus described in previous DTI studies was not statistically significant in the current study on 5 healthy adults which could be due to the small number of subjects. There is some debate as to whether the inability to trace the right arcuate fasciculus in some subjects reflects difficulties in diffusion tensor tractography in that region (Barrick and Clark 2004; Wahl et al. 2010; Yeatman at al. 2011) or reflects something more fundamental about the underlying neurobiology of language (Catani et al. 2007). Despite the small number of the cases, the major observations were consistent across all subjects. Our primary goal was to demonstrate feasibility of tracing the SLF fibers as has also been reported previously with a small number of subjects (Makris et al. 2005; Frey et al. 2008; Makris et al. 2009; Makris and Pandya 2009).

A relatively recent large probabilistic DTI study used automated approach for reconstruction of major brain pathways including the association tracts (Zhang et al. 2010). However, this study does not represent the SLF I, SLF II, superior and inferior parietal lobule connections of the adjacent language pathways described in the current study. Our description of regions of interest may be helpful for future probabilistic mapping of the SLF tracts in larger number of subjects using automated reconstruction and tract-specific quantification technique (Zhang et al. 2010). Better knowledge of detailed connectivity of the SLF combined with correlational functional studies could contribute to a better understanding and mapping of the human language network (Makris et al. 2005; Catani and Jones 2005; Frey et al. 2008; Makris et al. 2009). The current descriptions of the SLF fiber bundles provide basic anatomical information as the first step toward unraveling the detailed pathophysiology of the SLF including the SLF TP-SPL and MdLF-SPL in developmental disorders such autism (Fletcher et al. 2010; Poustka et al. 2012), schizophrenia (de Weijer et al. 2011), dyslexia (Ben-Shachar et al. 2007; Frye et al. 2010; Frye et al. 2011; Vandermosten et al. 2012), and acquired language or speech disorders (Catani et al. 2003; Catani and ffytche et al. 2005; Catani and Mesulam 2008; Breier et al. 2008; Shinoura et al. 2010; Turken and Dronkers 2011; Glasser and Rilling 2008; Fernández-Miranda et al. 2008).

Important research questions that pertain to the SLF may be pursued in future endeavors. For example, how do the SLF fiber bundles relative to brain gray matter domains vary with age across the human lifespan? And how do the SLF components relate to each other or vary with training, education, intervention and compensate in the presence of early developmental injury, or due to traumatic insults, lesions and tumors?

Conclusions

The current pilot study demonstrated the feasibility of high spatial resolution DTI data with sufficient sensitivity to elucidate more details of the pathways of the superior longitudinal fasciculi in the human brain. Our results are the first to present the whole superior longitudinal fasciculi macrostructural and microstructural architecture in relation to other language pathways serving as a step forward toward the detailed depiction of the human brain language network. Future technical advancements in high resolution DTI will permit the generation of detailed white matter maps of the language circuitry that may advance our understanding of disease processes affecting the language pathways.

Acknowledgments

This work is funded by the American National Institutes of Health (NIH)-Institute for Neurological Diseases and Stroke (NIH-NINDS: R01-NS052505-04) and the Dunn Research Foundation. The purchase of the 3.0 T MRI clinical scanner was partially funded by NIH grant S10 RR19186 awarded to Dr Ponnada A. Narayana. We wish to thank Vipul Kumar Patel for helping in data acquisition.

Abbreviations

AF	arcuate fasciculus
AG	angular gyrus
BA	Brodmann area
Cing	cingulum
DTI	diffusion tensor imaging
DTT	diffusion tensor tractography
DWI	diffusion weighted imaging
EmC	Extreme capsule
FA	fractional anisotropy
FACT	fiber assignment by continuous tracking
IFOF	inferior fronto-occipital fasciculus
ILF	Inferior longitudinal fasciculus
IPL	inferior parietal lobule
MD	mean diffusivity
MdLF	middle longitudinal fasciculus
ROI	region of interest
SLF	superior longitudinal fasciculus
SLF TP	temporoparietal portion of superior longitudinal fasciculus
SMG	supramarginal gyrus
SPL	superior parietal lobule
UF	Uncinate fasciculus
WM	white matter

References

1. Barrick TR, Clark CA. Singularities in diffusion tensor fields and their relevance in white matter fiber tractography. Neuroimage. 2004; 22:481–491. [PubMed: 15193577]
2. Ben-Shachar M, Dougherty RF, Wandell BA. White matter pathways in reading. Curr Opin Neurobiol. 2007; 17:258–270. [PubMed: 17379499]
3. Bernal B, Altman N. The connectivity of the superior longitudinal fasciculus: a tractography DTI study. Magn Reson Imaging. 2010; 28:217–225. [PubMed: 19695825]
4. Borra E, Belmalih A, Calzavara R, Gerbella M, Murata A, Rozzi S, Luppino G. Cortical connections of the macaque anterior intraparietal (AIP) area. Cereb Cortex. 2008; 18:1094–1111. [PubMed: 17720686]
5. Breier JI, Hasan KM, Zhang W, Men D, Papanicolaou AC. Language dysfunction after stroke and damage to white matter tracts evaluated using diffusion tensor imaging. AJNR Am J Neuroradiol. 2008; 29:483–487. [PubMed: 18039757]
6. Catani M, Piccirilli M, Cherubini A, Tarducci R, Sciarma T, Gobbi G, Pelliccioli G, Petrillo SM, Senin U, Mecocci P. Axonal injury within language network in primary progressive aphasia. Ann Neurol. 2003; 53:242–247. [PubMed: 12557292]
7. Catani M, ffytche DH. The rises and falls of disconnection syndromes. Brain. 2005; 128:2224–2239. [PubMed: 16141282]
8. Catani M, Mesulam M. The arcuate fasciculus and the disconnection theme in language and aphasia: history and current state. Cortex. 2008; 44:953–961. [PubMed: 18614162]
9. Catani M, Howard RJ, Pajevic S, Jones DK. Virtual in vivo interactive dissection of white matter fasciculi in the human brain. Neuroimage. 2002; 17:77–94. [PubMed: 12482069]
10. Catani M, Jones DK, ffytche DH. Perisylvian language networks of the human brain. Ann Neurol. 2005; 57:8–16. [PubMed: 15597383]
11. Catani M, Allin MP, Husain M, Pugliese L, Mesulam MM, Murray RM, Jones DK. Symmetries in human brain language pathways correlate with verbal recall. Proc Natl Acad Sci U S A. 2007; 104:17163–17168. [PubMed: 17939998]
12. de Weijer AD, Mandl RC, Diederen KM, Neggers SF, Kahn RS, Hulshoff Pol HE, Sommer IE. Microstructural alterations of the arcuate fasciculus in schizophrenia patients with frequent auditory verbal hallucinations. Schizophr Res. 2011; 130:68–77. [PubMed: 21641775]
13. Dubois J, Hertz-Pannier L, Cachia A, Mangin JF, Le Bihan D, Dehaene-Lambertz G. Structural asymmetries in the infant language and sensori-motor networks. Cereb Cortex. 2009; 19:414–423. [PubMed: 18562332]
14. Fernández-Miranda JC, Rhoton AL Jr, Alvarez-Linera J, Kakizawa Y, Choi C, de Oliveira EP. Three-dimensional microsurgical and tractographic anatomy of the white matter of the human brain. Neurosurgery. 2008; 62:989–1026. discussion 1026-8. [PubMed: 18695585]
15. Fletcher PT, Whitaker RT, Tao R, DuBray MB, Froehlich A, Ravichandran C, Alexander AL, Bigler ED, Lange N, Lainhart JE. Microstructural connectivity of the arcuate fasciculus in adolescents with high-functioning autism. Neuroimage. 2010; 51:1117–1125. [PubMed: 20132894]
16. Frye RE, Hasan K, Malmberg B, Desouza L, Swank P, Smith K, Landry S. Superior longitudinal fasciculus and cognitive dysfunction in adolescents born preterm and at term. Dev Med Child Neurol. 2010; 52:760–766. [PubMed: 20187879]
17. Frye RE, Liederman J, Hasan KM, Lincoln A, Malmberg B, McLean J 3rd, Papanicolaou A. Diffusion tensor quantification of the relations between microstructural and macrostructural indices of white matter and reading. Hum Brain Mapp. 2011; 32:1220–1235. [PubMed: 20665719]
18. Frey S, Campbell JS, Pike GB, Petrides M. Dissociating the human language pathways with high angular resolution diffusion fiber tractography. J Neurosci. 2008; 28:11435–11444. [PubMed: 18987180]
19. Galantucci S, Tartaglia MC, Wilson SM, Henry ML, Filippi M, Agosta F, Dronkers NF, Henry RG, Ogar JM, Miller BL, Gorno-Tempini ML. White matter damage in primary progressive aphasias: a diffusion tensor tractography study. Brain. 2011; 134:3011–3029. [PubMed: 21666264]

20. Glasser MF, Rilling JK. DTI tractography of the human brain's language pathways. Cereb Cortex. 2008; 18:2471–2482. [PubMed: 18281301]
21. Hains, DE. An Atlas of Structures, Sections and Systems. 7th ed.. New York: Lippincott Williams & Wilkins; 2007. Neuroanatomy.
22. Hasan KM, Kamali A, Kramer LA. Mapping the human brain white matter tracts relative to cortical and deep gray matter using diffusion tensor imaging at high spatial resolution. Magn Reson Imaging. 2009; 27:631–636. [PubMed: 19128910]
23. Hasan KM, Narayana PA. Computation of the fractional anisotropy and mean diffusivity maps without tensor decoding and diagonalization: theoretical analysis and validation. Magn Reson Med. 2003; 50:589–598. [PubMed: 12939767]
24. Hasan KM, Halphen C, Boska MD, Narayana PA. Diffusion tensor metrics, T2 Relaxation and volumetry of the naturally aging human caudate nuclei in healthy young and middle-aged adults: possible implications to the neurobiology of human brain aging and disease. Magn Reson Med. 2008; 59:7–13. [PubMed: 18050345]
25. Jang SH, Hong JH. The anatomical characteristics of superior longitudinal fasciculus I in human brain: Diffusion tensor tractography study. Neurosci Lett. 2012; 506:146–148. [PubMed: 22085696]
26. Jones DK. Studying connections in the living human brain with diffusion MRI. Cortex. 2008; 44:936–952. [PubMed: 18635164]
27. Kamali A, Kramer LA, Hasan KM. Feasibility of prefronto-caudate pathway tractography using high resolution diffusion tensor tractography data at 3T. J Neurosci Methods. 2010; 191:249–254. [PubMed: 20600311]
28. Koch G, Cercignani M, Pecchioli C, Versace V, Oliveri M, Caltagirone C, Rothwell J, Bozzali M. In vivo definition of parieto-motor connections involved in planning of grasping movements. Neuroimage. 2010; 51:300–312. [PubMed: 20156564]
29. Lebel C, Beaulieu C. Lateralization of the arcuate fasciculus from childhood to adulthood and its relation to cognitive abilities in children. Hum Brain Mapp. 2009; 30:3563–3573. [PubMed: 19365801]
30. Liu Y, Balériaux D, Kavec M, Metens T, Absil J, Denolin V, Pardou A, Avni F, Van Bogaert P, Aeby A. Structural asymmetries in motor and language networks in a population of healthy preterm neonates at term equivalent age: a diffusion tensor imaging and probabilistic tractography study. Neuroimage. 2010; 51:783–788. [PubMed: 20206706]
31. Luppino G, Murata A, Govoni P, Matelli M. Largely segregated parietofrontal connections linking rostral intraparietal cortex (areas AIP and VIP) and the ventral premotor cortex (areas F5 and F4). Exp Brain Res. 1999; 128:181–187. [PubMed: 10473756]
32. Makris N, Pandya DN. The extreme capsule in humans and rethinking of the language circuitry. Brain Struct Funct. 2009; 213:343–358. [PubMed: 19104833]
33. Makris N, Kennedy DN, McInerney S, Sorensen AG, Wang R, Caviness VS Jr, Pandya DN. Segmentation of subcomponents within the superior longitudinal fascicle in humans: a quantitative, in vivo, DT-MRI study. Cereb Cortex. 2005; 15:854–869. [PubMed: 15590909]
34. Makris N, Papadimitriou GM, Kaiser JR, Sorg S, Kennedy DN, Pandya DN. Delineation of the middle longitudinal fascicle in humans: a quantitative, in vivo, DT-MRI study. Cereb Cortex. 2009; 19:777–785. [PubMed: 18669591]
35. Mesulam MM. From sensation to cognition. Brain. 1998; 121:1013–1052. [PubMed: 9648540]
36. Mori S, van Zijl PC. Fiber tracking: principles and strategies — a technical review. NMR Biomed. 2002; 15:468–480. [PubMed: 12489096]
37. Petrides M, Pandya DN. Projections to the frontal cortex from the posterior parietal region in the rhesus monkey. J Comp Neurol. 1984; 228:105–116. [PubMed: 6480903]
38. Petrides M, Pandya DN. Comparative cytoarchitectonic analysis of the human and the macaque ventrolateral prefrontal cortex and corticocortical connection patterns in the monkey. Eur J Neurosci. 2002; 16:291–310. [PubMed: 12169111]
39. Poustka L, Jennen-Steinmetz C, Henze R, Vomstein K, Haffner J, Sieltjes B. Fronto-temporal disconnectivity and symptom severity in children with autism spectrum disorder. World J Biol Psychiatry. 2012; 13:269–280. [PubMed: 21728905]

40. Rozzi S, Calzavara R, Belmalih A, Borra E, Gregoriou GG, Matelli M, Luppino G. Cortical connections of the inferior parietal cortical convexity of the macaque monkey. Cereb Cortex. 2006; 16:1389–1417. [PubMed: 16306322]
41. Schmahmann JD, Smith EE, Eichler FS, Filley CM. Cerebral white matter: neuroanatomy, clinical neurology, and neurobehavioral correlates. Ann N Y Acad Sci. 2008; 1142:266–309. [PubMed: 18990132]
42. Schmahmann JD, Pandya DN, Wang R, Dai G, D'Arceuil HE, de Crespigny AJ, Wedeen VJ. Association fibre pathways of the brain: parallel observations from diffusion spectrum imaging and autoradiography. Brain. 2007; 130:630–653. [PubMed: 17293361]
43. Seltzer B, Pandya DN. Further observations on parieto-temporal connections in the rhesus monkey. Exp Brain Res. 1984; 55:301–312. [PubMed: 6745368]
44. Shinoura N, Onodera T, Kurokawa K, Tsukada M, Yamada R, Tabei Y, Koizumi T, Yagi K. Damage to the upper portion of area 19 and the deep white matter in the left inferior parietal lobe, including the superior longitudinal fasciculus, results in alexia with agraphia. Eur Neurol. 2010; 64:224–229. [PubMed: 20798545]
45. Turken AU, Dronkers NF. The neural architecture of the language comprehension network: converging evidence from lesion and connectivity analyses. Front Syst Neurosci. 2011; 5:1. [PubMed: 21347218]
46. Vandermosten M, Boets B, Poelmans H, Sunaert S, Wouters J, Ghesquière P. A tractography study in dyslexia: neuroanatomic correlates of orthographic, phonological and speech processing. Brain. 2012; 135(Pt 3):935–948. [PubMed: 22327793]
47. Wahl M, Li YO, Ng J, Lahue SC, Cooper SR, Sherr EH, Mukherjee P. Microstructural correlations of white matter tracts in the human brain. Neuroimage. 2010; 51:531–541. [PubMed: 20206699]
48. Wedeen VJ, Wang RP, Schmahmann JD, Benner T, Tseng WY, Dai G, Pandya DN, Hagmann P, D'Arceuil H, de Crespigny AJ. Diffusion spectrum magnetic resonance imaging (DSI) tractography of crossing fibers. Neuroimage. 2008; 41:1267–1277. [PubMed: 18495497]
49. Yeatman JD, Dougherty RF, Rykhlevskaia E, Sherbondy AJ, Deutsch GK, Wandell BA, Ben-Shachar M. Anatomical properties of the arcuate fasciculus predict phonological and reading skills in children. J. Cogn. Neurosci. 2011; 23:3304–3317. [PubMed: 21568636]
50. Zhang Y, Zhang J, Oishi K, Faria AV, Jiang H, Li X, Akhter K, Rosa-Neto P, Pike GB, Evans A, Toga AW, Woods R, Mazziotta JC, Miller MI, van Zijl PC, Mori S. Atlas-guided tract reconstruction for automated and comprehensive examination of the white matter anatomy. Neuroimage 1. 2010; 52:1289–1301.

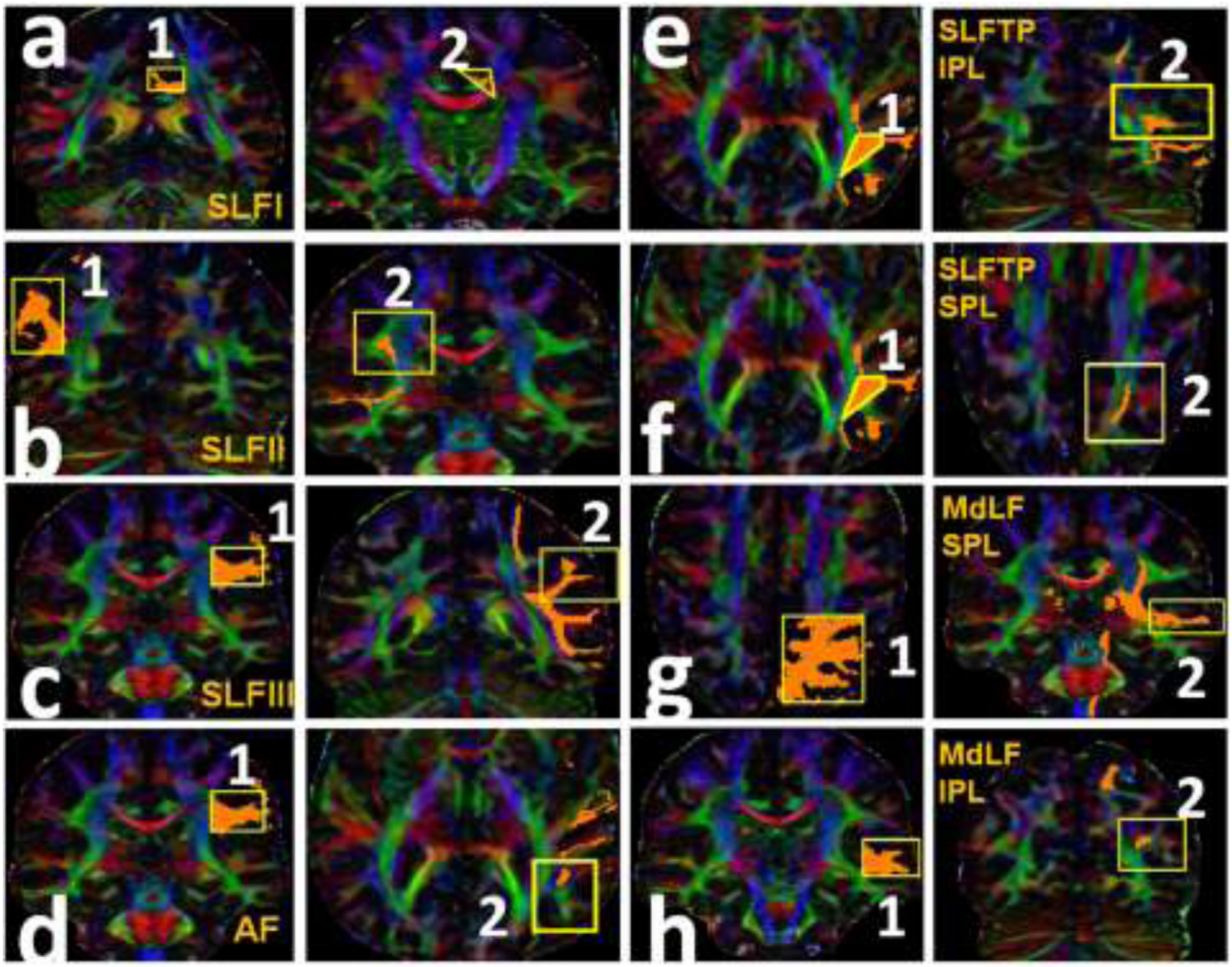

Figure1.

The selected ROI seeds (ROI 1 and ROI 2) for each language fiber tract are illustrated. The detailed description of the planes and ROIs for each tract is in the methods section. (a) SLF I: the ROI 1 is delineated over the green association bundles just superolateral to the cingulum. The ROI 2 was placed over the fibers generated on the superolateral aspect of the cingulum. (b) SLF II: the ROI 1 is placed over the white matter of the angular gyrus (coronal plane e in Figure 2). The second ROI was placed on the fibers generated on the association green area. (c) SLF III: the ROI 1 is paced over the periventricular green association fibers followed by the second ROI over the fibers generated on the white matter of the supramarginal gyrus (d) AF: the first ROI is the same as ROI 1 for the SLF III. The ROI 2 is situated over the periventricular craniocaudally oriented blue fibers. (e) SLF TP-IPL: the first ROI was selected on the periventricular blue fibers lateral to the green association fibers followed by seeding the second ROI on the fibers generated on the inferior parietal lobule. (f) SLF TP-SPL: the first ROI is the same as ROI 1 for SLF TP-IPL. The ROI 2 is seeded over the fibers generated at the centrum semiovale. (g) MdLF-SPL: the ROI 1 is selected over the ascending blue fibers of the parietal cortex and the ROI 2 on the fibers generated in the superior temporal gyrus. (h) MdLF-IPL: the ROI1 was selected on the

superior temporal gyrus, followed by placing the second ROI on the fibers generated at the parietooccipital confluence.

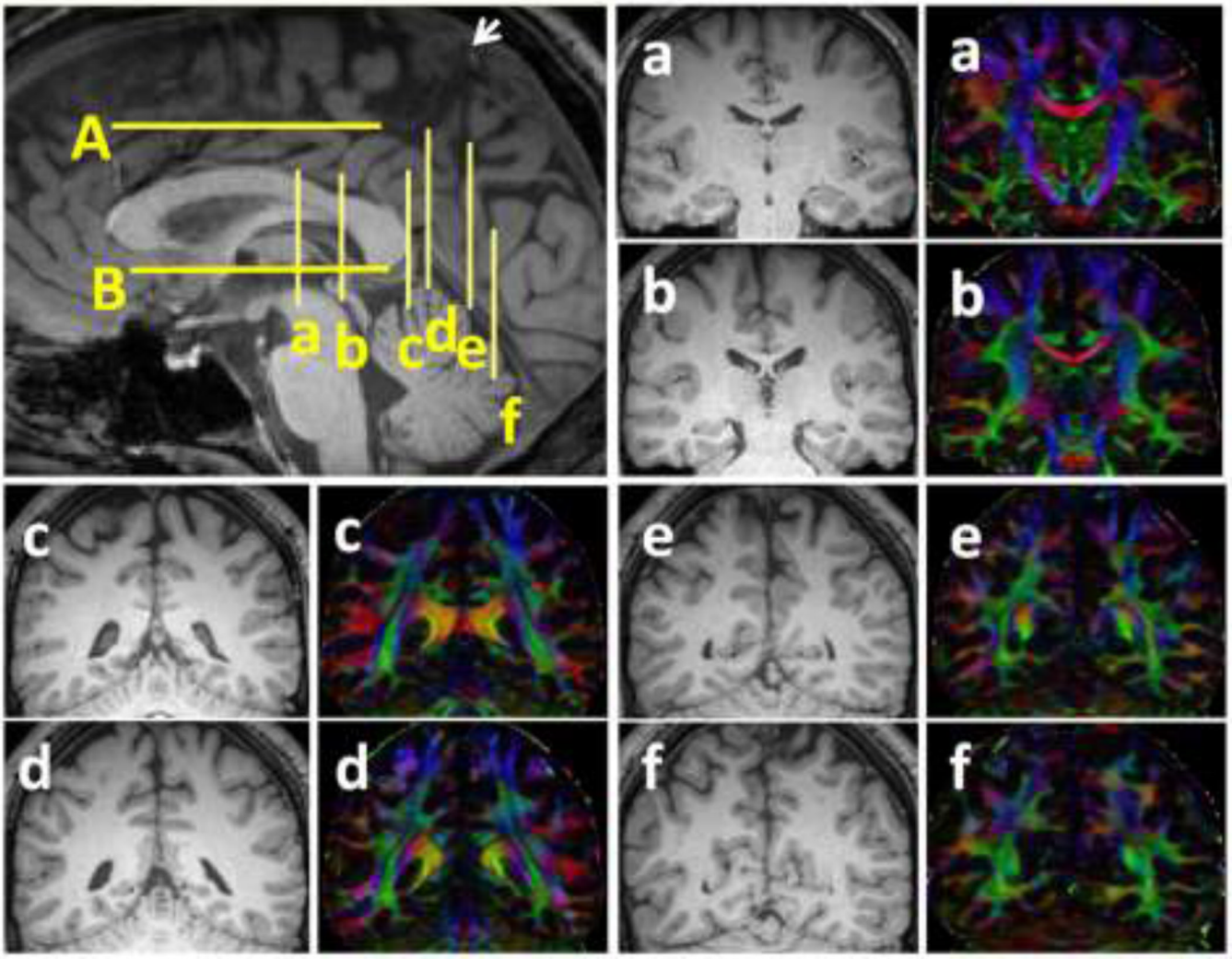

Figure 2.

Structural (T1-weighted) MRI of the sagittal midline plane showing the corresponding axial and coronal planes used for ROI placement in figure 1. The corresponding T1-weighted and diffusion tensor color-coded map of the coronal sections of a–f are also provided.

(a) The coronal plane a is at the midthalamic, coronal plane b is at the posterior-most portion of the fornix on the midline plane, coronal plane c is at the posterior-most coronal level of the corpus callosum, coronal plane d is at the confluence of the superior ramus and the cingulate sulcus, coronal plane e is at the cortical origin of the ramus of the cingulate sulcus and the coronal plane f is at the caudal end of the parietooccipital sulcus in the midsagittal cut. (b) The axial plane A is at the level of the cingulate sulcus, axial plane B is at the level of the anterior commissure.

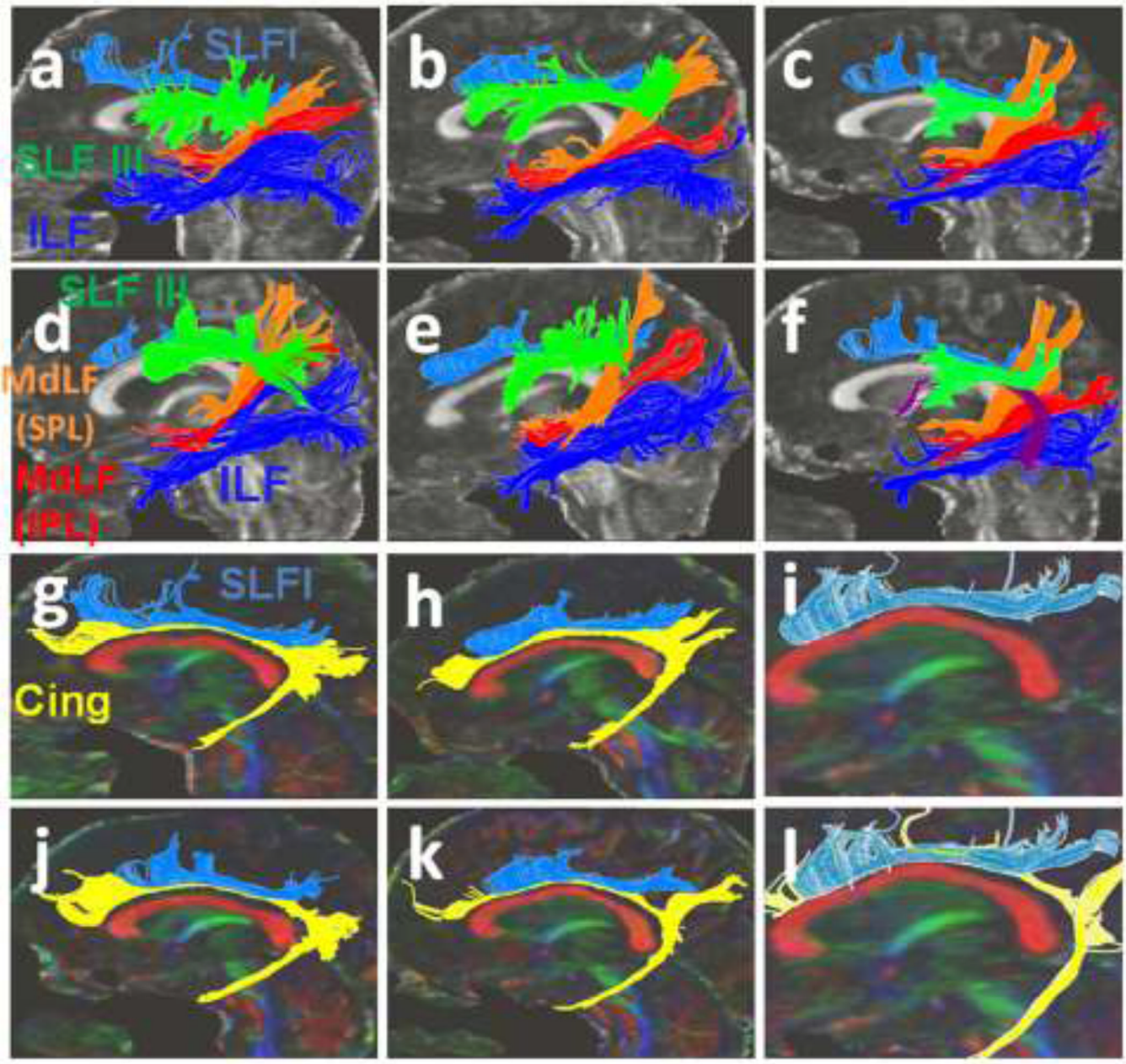

Figure 3.

(3a–e) Three-dimensional reconstructions of the SLF I (light blue), SLF III (green), MdLF (inferior parietal lobule connection in red and superior parietal lobule connection in orange color), ILF (dark blue) and Cingulum (Cing in yellow) for five individuals were portrayed. (3f) The arcuate fasciculus is shown in maroon color in one of the subjects. (3g–l) The SLF I (light blue) and the cingulum (yellow) are imaged in five subjects.

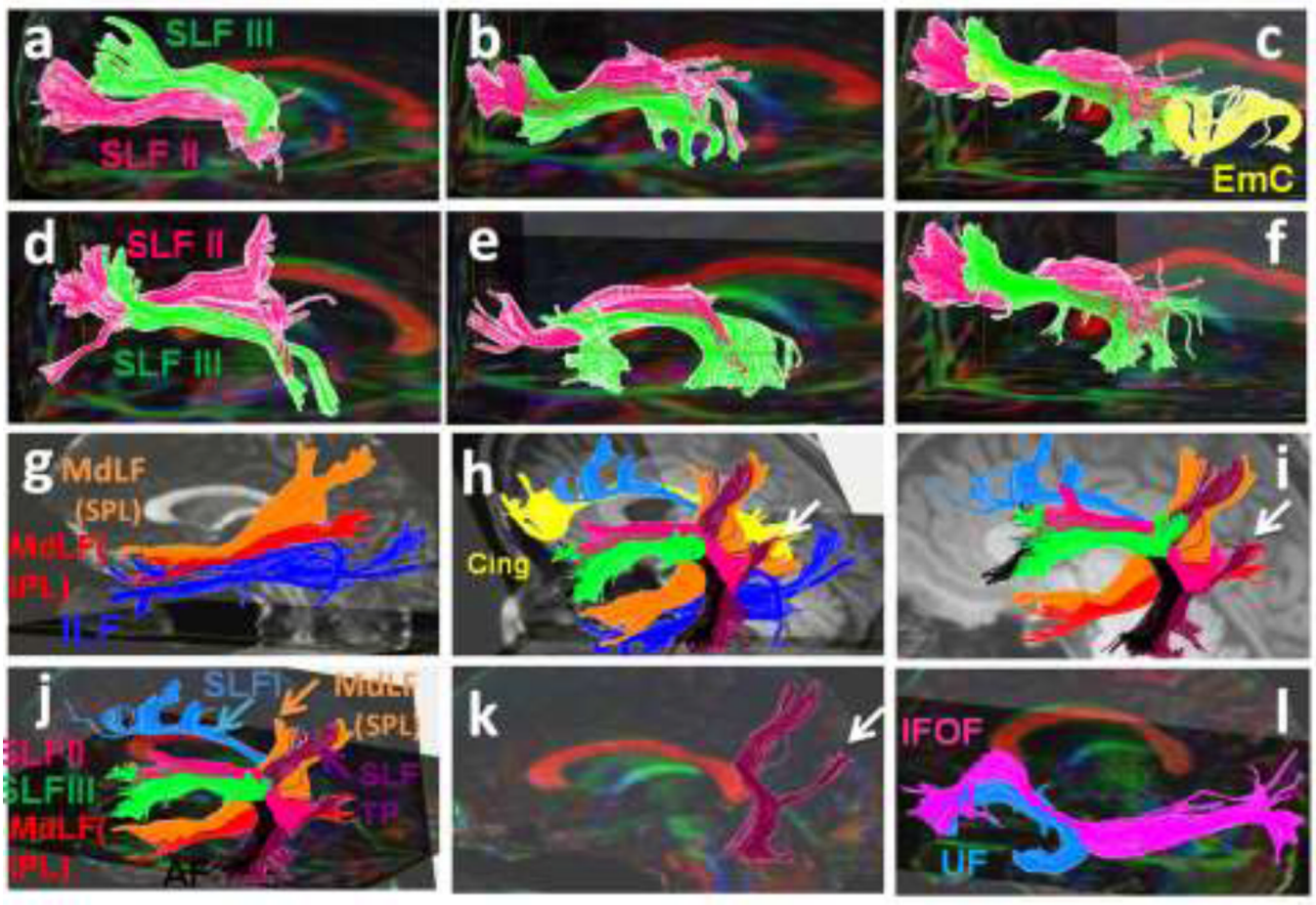

Figure 4.

(a–f) Three-dimensional reconstructions of the SLF II (pink), and SLF III (green) created for each individual are shown. Trajectory of the extreme capsule (EmC) (yellow in 4c) as well as the relationship of the SLF II and SLF III with extreme capsule in one of the subjects is shown in Figure 4c. (g) The inferior parietal lobule connection of the MdLF (MdLF-IPL in red color) and the superior parietal lobule connection of the MdLF (MdLF-SPL in orange color) and the ILF (dark blue) are demonstrated. (4h–l) The relationship of the SLF II and SLF III with other adjacent association fibers such as the cingulum (yellow), SLF I (light blue), ILF (dark blue), AF (black) and temporoparietal portion of the SLF (SLF TP in purple color) are illustrated. In figure 4h the SLF TP-IPL and SLF TP-IPL are combined together and are assigned the orange color. (k) The trajectory of the SLF TP is portrayed. The angular gyrus (inferior parietal lobule) connections of the SLF TP are demonstrated by the arrows (h–k). The superior parietal connections are also shown. (l) The IFOF (pink) and the UF (green) in one of the subjects are illustrated.

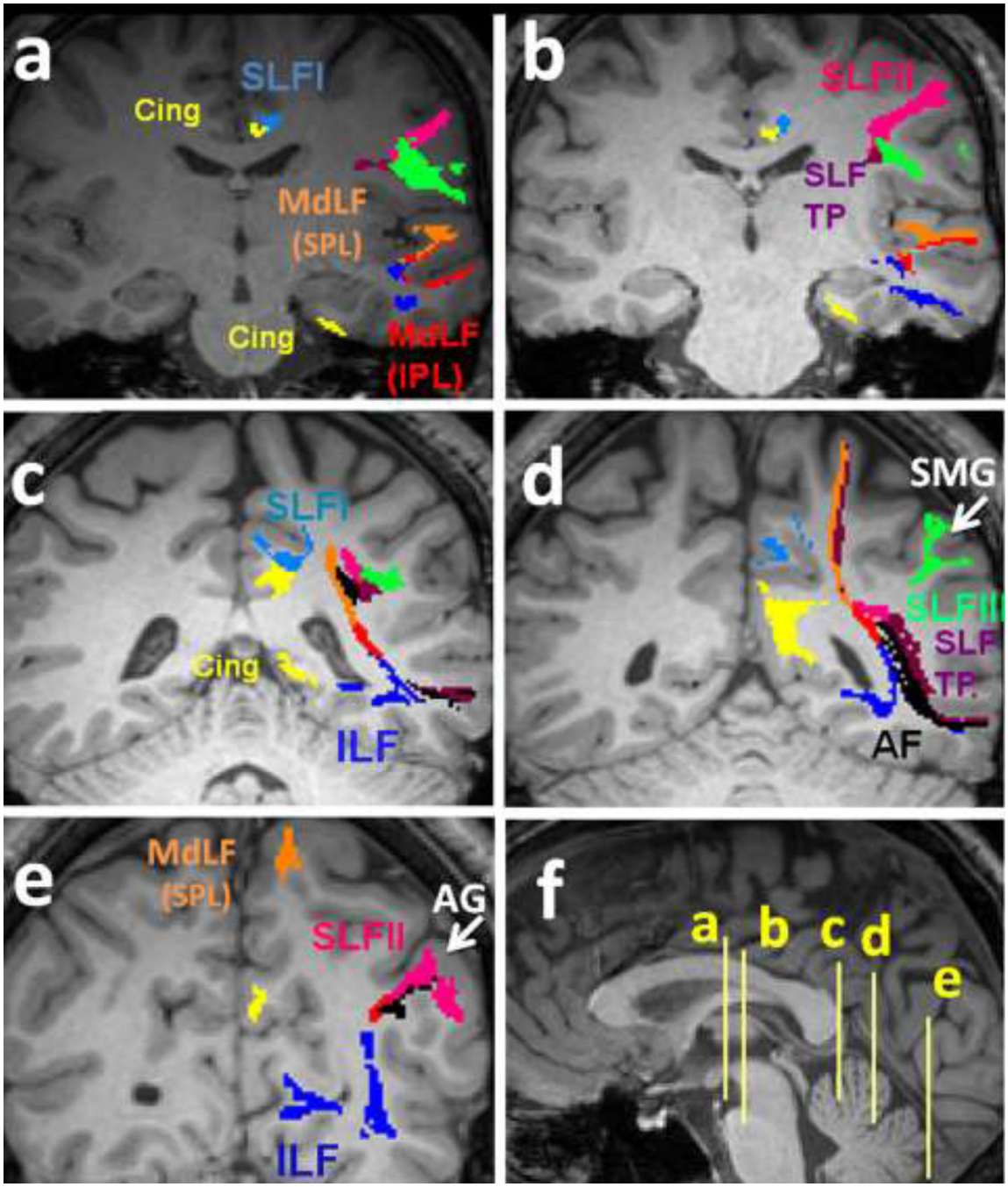

Figure 5.

Five consecutive coronal T1 images show a detailed description of the language pathways. Please attention that the color-coding is fixed across all the images. The coarse trajectories of the SLF I (light blue), SLF II (pink), SLF III (green), SLF TP (purple), MdLF (inferior parietal lobule connection in red and superior parietal lobule connection in orange color), ILF (dark blue), Cingulum (yellow) and AF (black) for one individual are illustrated. Corresponding axial planes are demonstrated in mid sagittal cut in Figure 5f.

Table 1

Summary and comparison of the group average and standard deviation of the SLF tract volumes and corresponding diffusion tensor fractional anisotropy (FA) and average diffusivity (D_{av}) in both hemispheres.

		Left	Right	p
Tract Volume(ml)	SLF I	2.418 ± 0.866	2.979 ± 1.770	0.34
	SLF II	3.692 ± 2.577	5.007 ± 2.177	0.13
	SLF III	3.352 ± 0.818	4.406 ± 0.789	0.08
	AF	5.766 ± 2.228	5.665 ± 3.355	0.15
	TP slf	3.769 ± 1.633	2.427 ± 1.688	**0.06**
	MdLF SPL	3.715 ± 2.097	4.967 ± 1.019	0.14
	MdLF IPL	3.014 ± 1.663	2.964 ± 1.134	0.95
FA	SLF I	0.494 ± 0.016	0.476 ± 0.015	0.09
	SLF II	0.451 ± 0.023	0.444 ± 0.086	0.35
	SLF III	0.451 ± 0.035	0.459 ± 0.020	0.37
	AF	0.496 ± 0.032	0.475 ± 0.022	0.06
	TP slf	0.463 ± 0.022	0.448 ± 0.013	**0.05**
	MdLF SPL	0.466 ± 0.026	0.444 ± 0.022	**0.05**
	MdLF IPL	0.456 ± 0.021	0.458 ± 0.018	0.87
Mean Diffusivity ($\times 10^{-3}$ mm^2 sec^{-1})	SLF I	0.833 ± 0.024	0.830 ± 0.024	0.95
	SLF II	0.827 ± 0.028	0.853 ± 0.045	0.1
	SLF III	0.853 ± 0.018	0.853 ± 0.030	0.92
	AF	0.833 ± 0.024	0.832 ± 0.01	0.19
	TP slf	0.840 ± 0.028	0.827 ± 0.043	0.37
	MdLF SPL	0.873 ± 0.028	0.887 ± 0.018	0.18
	MdLF IPL	0.880 ± 0.018	0.867 ± 0.023	0.48

Whole brain WM volume ~ 866.80 ± 8.6 (mL)
Percentage of whole SLF white matter tract volume to whole brain white matter volume ~ 4.28 ± 0.62 %